Chemical Physics Letters 590 (2013) 208–213

Contents lists available at ScienceDirect

Chemical Physics Letters

journal homepage: www.elsevier.com/locate/cplett

Artifacts due to trivial unavoided crossings in the modeling of photoinduced energy transfer dynamics in extended conjugated molecules

Tammie Nelson [a], Sebastian Fernandez-Alberti [b], Adrian E. Roitberg [c,d], Sergei Tretiak [a,*]

[a] Theoretical Division, Center for Nonlinear Studies (CNLS), Center for Integrated Nanotechnologies (CINT), Los Alamos National Laboratory, Los Alamos, NM 87545, USA
[b] Universidad Nacional de Quilmes, Roque Saenz Peña 352, B1876BXD Bernal, Argentina
[c] Department of Physics, Quantum Theory Project, University of Florida, Gainesville, FL 32611, USA
[d] Department of Chemistry, Quantum Theory Project, University of Florida, Gainesville, FL 32611, USA

ARTICLE INFO

Article history:
Received 22 July 2013
In final form 17 October 2013
Available online 24 October 2013

ABSTRACT

A previously developed algorithm to identify potential energy surface crossings involving interacting or noninteracting states during nonadiabatic excited-state molecular dynamics simulations, allows the diabatic pathway to be followed through the crossing region so that there is no experienced change in the states identity. In this Letter, we investigate the transition from interacting/delocalized states to noninteracting/localized states in oligomers of poly-phenylene vinylene separated by varying distances. We demonstrate that the appearance of trivial unavoided crossings during nonadiabatic dynamics leads to artifacts in the state population analysis. Consequently, changes in the localization of the electronic transition density must be followed instead.

1. Introduction

Excited state molecular dynamics of any polyatomic molecular system [1–3] is likely to experience multiple regions of potential energy surface (PES) crossings within its excited state lifetime [4]. Consequently, either weakly or strongly avoided crossings, as well as unavoided crossings are common events during radiationless vibronic relaxation [5–10]. Conical intersections dominate nonadiabatic nuclear dynamics on very short (femtosecond) timescales [4]. In extended polyatomic molecules, special cases of unavoided crossings can also take place between two noninteracting states occupying the same energy range while different moieties are spatially separated and their wavefunctions have vanishing interactions. In such cases, denoted as trivial unavoided crossings, the nonadiabatic couplings behave as sharp peaks strongly localized at the exact crossing points while vanishing elsewhere. Here the wavepacket trajectory must cross the conical intersection seam following the diabatic pathway of its parent wavefunction along the respective adiabatic PES. Failure to follow the correct pathway can lead to unphysical sudden changes in the spatial localization of the current state [11].

Within the domain of small and medium sized molecules, at least within some regions of phase space, intramolecular excited states that are close in energy will commonly interact with one another. As a consequence, these states mix and cross, their identities temporarily change, and electronic population is transferred between them. Because of that, the use of energy ordering to identify the states becomes useless and adiabatic state populations lose their relevance. Instead, changes in the electronic transition density must be followed. Similar behavior can be expected between electronic excited states belonging to similar molecules separated by short intermolecular distances. Nevertheless, while states on two different molecules or on two separate fragments within the same molecule may be interacting at short separation distances, they become noninteracting when the separation distance increases.

In this Letter, we analyze the transition from interacting to noninteracting states, which can lead to the appearance of trivial unavoided crossings during dynamics. As was recently demonstrated by our group, these crossings play a critical role in the dynamics of organic conjugated polymers. For example, during energy transfer dynamics in PPV oligomers, torsional fluctuations can cause excited state energy reordering [12]. Failure to detect such crossings can lead to unphysical population transfer between electronic states and an apparently high efficiency of energy transfer [11]. Here, we address artifacts observed when analyzing the populations of adiabatic electronic excited states. These artifacts are associated with the incidence of trivial unavoided crossings, and we discuss how they vanish when the number of trivial unavoided crossings during photoinduced dynamics decreases.

* Corresponding author. Fax: +1 505 665 4063.
E-mail address: serg@lanl.gov (S. Tretiak).

0009-2614/$ - see front matter © 2013 Elsevier B.V. All rights reserved.
http://dx.doi.org/10.1016/j.cplett.2013.10.052

2. Theoretical methodology

2.1. Nonadiabatic excited-state molecular dynamics

We have performed Nonadiabatic Excited-State Molecular Dynamics (NA-ESMD) simulations [13] of the photoexcited dynamics in the model system depicted in Figure 1A composed of 3-ring and 4-ring poly-phenylene vinylene (PPV) oligomers. The NA-ESMD formalism combines the fewest switches surface hopping (FSSH) approach [14,15] with "on the fly" analytical calculations of excited state energies [16,17], gradients [18], and nonadiabatic coupling terms (NACTs) [13,19,20] in order to simulate photoinduced dynamics in large conjugated organic molecules involving many coupled electronic excited states on time scales of tens of picoseconds [21,22,2,23]. Correlated excited states are described using the Collective Electronic Oscillator (CEO) method [24–26] applied at the Austin Model 1 (AM1) [27] level of theory in combination with a Configuration Interaction Singles (CIS) formalism. At any given time, the nuclei are evolved on a single adiabatic PES, and transitions between coupled electronic states are possible depending on the nonadiabatic coupling strength [28]. Although dielectric medium effects are not explicitly included in the excited state calculations underlying our MD simulations, a phenomenological description of solvent effects is included in the nuclear propagation through the use of constant-temperature Langevin dynamics algorithm [29] developed to be consistent with the velocity Verlet integration technique [30] incorporating frictional damping and a fluctuating force following the fluctuation–dissipation theorem [31]. Details of NA-ESMD implementation and limitations can be found in our previous work [13,32].

2.2. Min-Cost identification of unavoided crossings

We have recently developed a novel procedure to identify crossing events by tracking the identities of states over time. Using the so-called Min-Cost assignment algorithm, new states at the current time step i can be assigned in terms of old states at the preceding time step $(i-1)$. The correspondence between states is found at each time step based on maximizing the trace of the square of the overlap matrix, $\mathbf{S}$, whose elements are defined as

$$s_{\alpha\beta}(t;t+\Delta t) \equiv \phi_\beta(\mathbf{r};\mathbf{R}(t)) \cdot \phi_\alpha(\mathbf{r};\mathbf{R}(t+\Delta t)) \quad (1)$$

where ϕ_α and ϕ_β are the adiabatic electronic state wavefunctions, $\mathbf{r}$ and $\mathbf{R}$ represent electronic and nuclear coordinates, respectively, and Δt is the classical time step used for NA-ESMD simulations. This is done by selecting one element from each row, each pertaining to a different column (or vice versa), from the matrix $\mathbf{S}(t;t+\Delta t)$ such that the sum of their squared values is maximized. If a maximum overlap greater than an arbitrary threshold, s_{lim}, is identified, then the states are reassigned by interchanging their populations and cancelling their couplings without evaluating the hopping probability. This removes the arbitrary effect of the nonadiabatic coupling strength depending on the proximity to the exact crossing point. Thus, unavoided crossings involving interacting states (simulated by quantum hops) can be differentiated from trivial unavoided crossings between noninteracting states (detected by tracking state identities). Further details of its implementation within the NA-ESMD [13] framework are provided elsewhere [11].

2.3. Simulation details

The separation distance, r_{CM}, is defined as the distance between the centers of mass of each oligomer and is varied according to Ta-

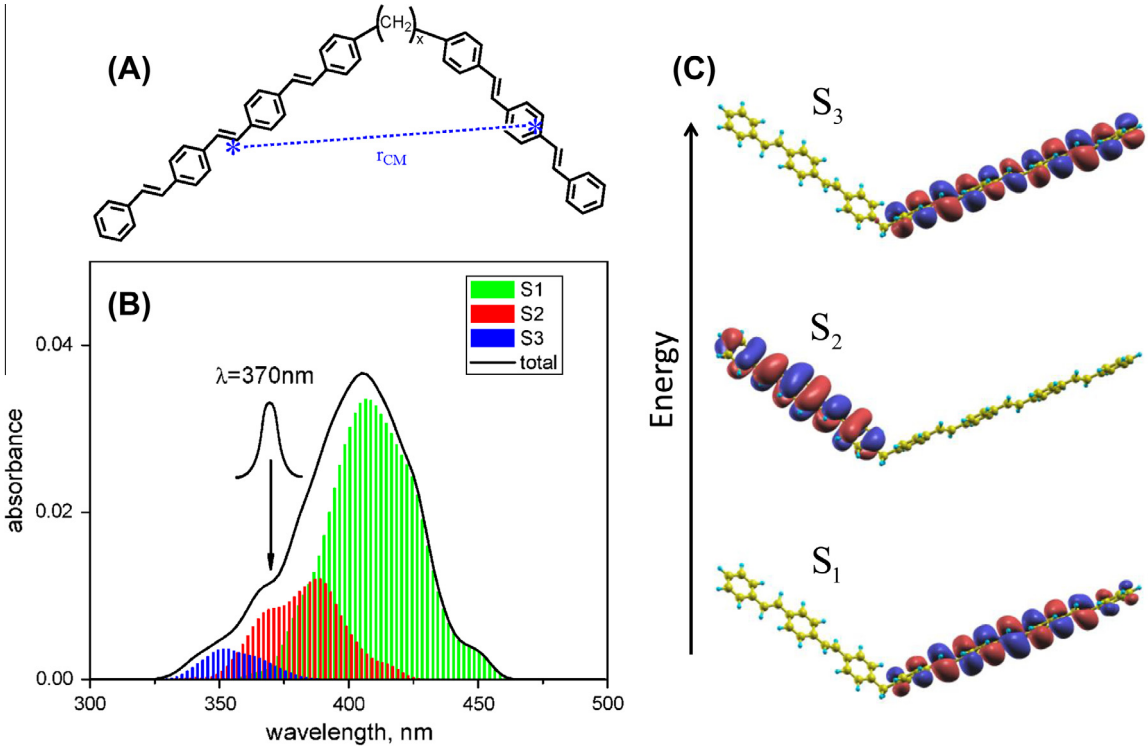

Figure 1. (A) Chemical structure of 3-ring and 4-ring PPV segments connected by an alkyl chain of length x (C_xH_{2x}). r_{CM} defines the separation distance between the centers of mass of the two segments. For larger separation distances, the alkyl chain is removed. (B) Simulated absorption spectrum for the $x = 1$ (19 Å) system (black line) and the density of excited states (sticks). The arrow indicates the maximum excitation wavelength used to populate the initial excited states. (C) Initial transition density localization for the three lowest energy excited electronic states.

ble 1. For systems linked by an alkyl chain of length x (C_xH_{2x}), a ground-state molecular dynamics trajectory was performed for 650 ps with a friction coefficient of 2.0 ps^{-1} at 300 K starting from an AM1 optimized structure. Snapshots were collected from the ground-state trajectory at 500 fs intervals representing a thermally equilibrated ensemble to provide the initial positions and momenta for subsequent excited state simulations. In order to create larger separation distances (50 Å, 200 Å), the alkyl chain from the $x = 1$ snapshots was replaced by a terminal hydrogen atom at the end of each segment. Segments were then separated to the desired distance by increasing r_{CM} along the center of mass vector, and the resulting geometries were relaxed by an additional 50 fs of ground-state MD.

In conjugated organic polymers, such as poly-phenylene vinylene (PPV), linear segments of varying lengths can act as weakly coupled chromophore units. Therefore, the total absorption spectrum can be interpreted as the sum of the contributions from each fragment with strong overlap between the component spectra [21,23]. The total absorption spectrum for the $x = 1$ (19 Å) system is shown in Figure 1B along with the density of excited states (DOES). The DOES is a histogram of the excited state energies calculated for each of the initial NA-ESMD configurations, the height of which is weighted by the average oscillator strength for the respective state. Clearly, from the overlapping DOES, multiple states occupy the same energy range and trivial unavoided crossings are expected to be prevalent in this system. The initial localization of the transition density is shown in Figure 1C for the AM1 optimized planar ground-state geometry. The lowest energy excited state, S_1, is localized on the 4-ring segment. The second state, S_2, has transition density localized on the 3-ring fragment while the third state is localized on the 4-ring side, S_3.

The initial excited state was chosen according to a Frank–Condon window defined as

$$g_\alpha(\mathbf{r},\mathbf{R}) = exp[-T^2(E_{laser} - \Omega_\alpha)^2], \tag{2}$$

where E_{laser} represents the energy of a laser centered at λ=370 nm and Ω_α represents the energy of state α from the theoretical absorption spectrum. The laser shape is assumed to be Gaussian $f(t) = exp(-t^2/2T^2)$, T^2=42.5 fs corresponding to a FWHM of 100 fs. The initial excitation is selected according to the relative values of $g_\alpha(\mathbf{r},\mathbf{R})$ weighted by the oscillator strengths of each state α. In this way, the initial excitation corresponds to S_3 or S_2. An ensemble of 1080 independent NA-ESMD trajectories was propagated for 500 fs at 300 K where 5 electronic excited states and their nonadiabatic coupling vectors have been included. The nuclei were propagated with a classical time step of $\Delta t = 0.1$ fs, with N_q = 10 quantum time steps per classical step for the evaluation of the nonadiabatic couplings and propagation of the quantum coefficients. The quantum time step was further reduced by a factor of 40 for the detection of possible trivial unavoided crossings [11]. The number of converged trajectories for each system is provided in Table 1.

Table 1
Separation distances between 3-ring and 4-ring PPV segments for the ground state AM1 optimized systems, the number of converged excited-state trajectories for each system, and the number of trajectories initially in a mixed state.

x (C_xH_{2x})	r_{CM}, Å	Converged	Mixed
x = 1	19.5	1021	208
x = 5	24.5	976	71
x = 11	31.1	1020	23
–	50	1077	12
–	200	1077	6

3. Results

3.1. From interacting/delocalized to noninteracting/localized states

The degree of exciton delocalization is related to the strength of electronic coupling between the segments. In cases of strong coupling, where electronic states on either segment are interacting, the excitation may be delocalized over both oligomers. For noninteracting states, the lack of electronic coupling between the segments localizes the excitation. Following [11,12], we characterize delocalization of the electronic states using the transition density matrix, $(\rho^{g\alpha})_{nm}$, representing net changes in the distribution of the electronic density matrix induced by an optical excitation from the ground state g to an excited electronic state α [24,33]. $(\rho^{g\alpha})_{nm}$ is also the CIS eigenvector with a natural normalization condition $\sum_{nm}(\rho^{g\alpha})^2_{nm} = 1$, where n and m run over the basis functions. The transition density fractions $(\rho^{g\alpha})^2_{3-ring}$ and $(\rho^{g\alpha})^2_{4-ring}$ localized on 3-ring and 4-ring PPV segments, respectively, are obtained by summing the contributions from each atom belonging to the segment. In the following, we use the simplified notation $(\rho^{g\alpha})^2_{X-ring}$ (X = 3,4) where X counts the number of monomers on each oligomer.

By considering the localization of the initial excitation (at time $t = 0$), we observe very different behavior for the various separation distances. A simple inspection of the number of mixed states listed in Table 1 (when the initial transition density is described by $0.20 < (\rho^{g\alpha})^2_{X-ring} < 0.80$ for either oligomer) reveals that states with mixed character are more common at short distances becoming less probable with increasing separation distance. This trend is also revealed by examining the participation number [21,23,34] (inverse of the participation ratio first defined by Thouless, Dean, and Bell [35,36]), which represents the extent of (de) localization of an excitation given by

$$P = \left[\sum_X ((\rho^{g\alpha})^2_{X-ring})^2\right]^{-1} \tag{3}$$

where X = 3,4. We calculate the participation number *per segment* where $1 \leqslant P \leqslant 2$. Here $P = 1$ indicates localization to a single segment while $P = 2$ corresponds to a complete delocalization over both oligomers. Histograms of the participation number for the initial excitations, P($t = 0$), calculated using all initial snapshots of converged trajectories, are shown in the top panel of Figure 2. At short distances, there is some probability that the excitation will be delocalized over more than one segment, indicated by a long tail in the distribution extending to $P = 2$. This tail corresponds to the relatively large fraction of mixed states from Table 1 for the shortest distances. However, excitations quickly become localized to a single segment as the distance increases, and the distribution tail vanishes along with the number of mixed states.

The nonadiabatic coupling terms (NACTs) are defined as $\dot{\mathbf{R}} \cdot \mathbf{d}_{\alpha\beta} = \langle\phi_\alpha|\frac{\partial\phi_\beta}{\partial t}\rangle$, and the nonadiabatic coupling vector is given by $\mathbf{d}_{\alpha\beta} = \langle\phi_\alpha(\mathbf{R})|\nabla_{\mathbf{R}}\phi_\beta(\mathbf{R})\rangle, \alpha \neq \beta$. A histogram of the NACTs between S_1 and S_2 during NA-ESMD simulations is shown in the bottom panel of Figure 2 for each separation distance. The height of the histograms corresponds to the fraction of NACTs between S_1 and S_2 with the given value where NACTs computed every 0.1 fs along all converged trajectories have been included. States separated by short distances are strongly interacting, indicated by a broad NACT distribution. As the segments are separated, the localized states have vanishing interactions.

3.2. Appearance of trivial unavoided crossings

While interacting states give rise to conical intersections, noninteracting states can result in the appearance of trivial unavoided crossings. Although there is no interaction between them, a diabatic state $S_n^{(d)}$ may cross energetically below state $S_{n-1}^{(d)}$ when the

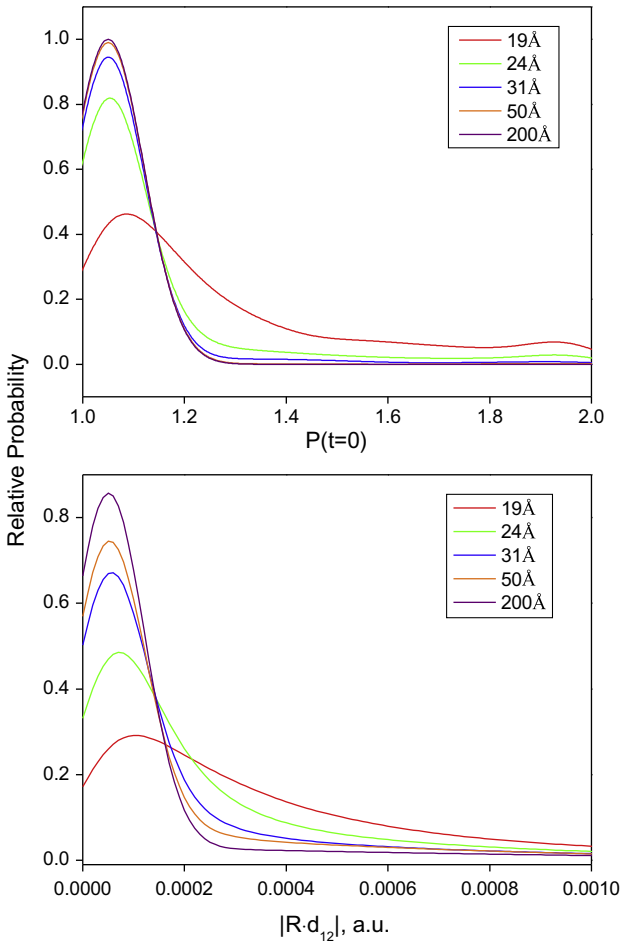

Figure 2. (Top) Histograms of the participation number (per segment) for the initial configurations at each separation distance. $P = 1$ ($P = 2$) corresponds to complete localization (delocalization) of the initial excitation. The initial excitation goes from being delocalized to being localized on a single oligomer with increasing separation distance. (Bottom) Histograms of NACT between S_2 and S_1 states. A significant coupling between the interacting states, present at short separations, vanishes at larger separation distances.

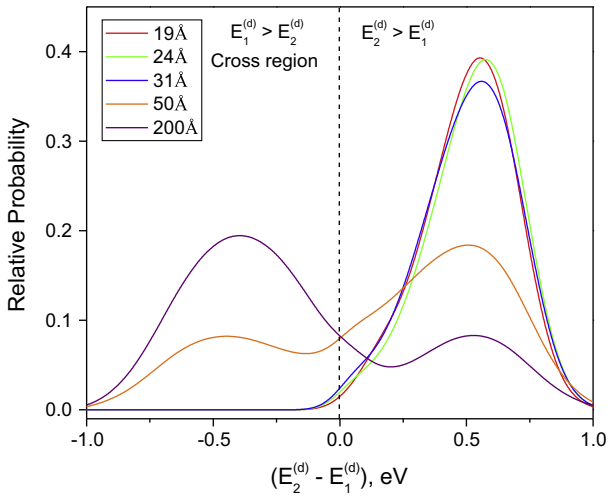

Figure 3. Histograms of the energy gap $\Delta E_{12}^{(d)} = E_2^{(d)} - E_1^{(d)}$ between diabatic $S_2^{(d)}$ and $S_1^{(d)}$ states. The crossing region corresponds to times when $S_2^{(d)}$ is energetically below $S_1^{(d)}$ following a trivial unavoided cross. For the shortest separation distances, the system has a positive energy separation ($E_2^{(d)} > E_1^{(d)}$) consistent with the initial energy ordering. As the separation distance increases, the probability of negative energy separation ($E_1^{(d)} > E_2^{(d)}$) increases as $S_2^{(d)}$ and $S_1^{(d)}$ cross each other.

two states occupy the same energy range. For clarity, we introduce the notation $S_n^{(d)}/S_n^{(a)}$ where (d/a) indicates *diabatic*/*adiabatic* representation and n refers to the initial energy ordering at time t = 0. The energy gap between $S_1^{(d)}$ and $S_2^{(d)}$ states ($\Delta E_{12}^{(d)} = E_2^{(d)} - E_1^{(d)}$) measures the energy ordering of the states. Using the identities of the initial (t = 0) $S_1^{(d)}$ and $S_2^{(d)}$ states as templates, $\Delta E_{12}^{(d)} > 0$ when $S_2^{(d)}$ remains at higher energy than $S_1^{(d)}$. Following a cross, $S_2^{(d)}$ will be at lower energy than $S_1^{(d)}$ and $\Delta E_{12}^{(d)} < 0$. A histogram of the energy gap $\Delta E_{12}^{(d)}$ during the 500 fs dynamics is shown in Figure 3 for each separation distance. Here the energy gaps are sampled every 0.1 fs along each converged trajectory. For small separation distances, the energy gap is always positive ($E_2^{(d)} > E_1^{(d)}$) indicating that strongly interacting states do not cross each other (i.e., the original energy ordering is preserved). At large separation distances, where interaction vanishes, we observe a decrease in the probability of positive energy gap and a concomitant increase in the probability of negative energy gaps ($E_2^{(d)} < E_1^{(d)}$). Therefore, in these cases, the system spends more time in the reversed energy ordering regime due to the appearance of crosses between $S_2^{(d)}$ and $S_1^{(d)}$. Clearly, the system remains in the 'crossed regime' for an overall larger amount of time at longer distances. There can be two causes for this observation (1) at larger distances there are longer time intervals between the initial crossing event and recrossing to the original energy ordering, or (2) crosses become more prevalent at longer distances.

In the first case, a decrease in the number of crosses with separation distance is expected in order for the reversed energy ordering to be preserved for a longer time before recrossing. However, according to our observations, case (2) is the correct interpretation. The top panel of Figure 4 shows the number of trivial unavoided crosses between $S_1^{(d)}$ and $S_2^{(d)}$ in 5 fs increments during the 500 fs dynamics for various separation distances. The height of the histogram represents the number of crosses in the ensemble of converged trajectories. Trivial unavoided crossings are absent in the systems separated by short distances (when states are interacting) and appear only for the largest separation distances (50 Å and 200 Å). The number of crosses grows as the separation is increased and the interaction between the states begins to vanish (see NACTs in bottom panel of Figure 2). Therefore, at larger distances, there is an overall increase in the number of crossing events rather than an increase in the length of each crossing event. Indeed, only the relative heights of the peaks change in Figure 4 rather than their positions.

3.3. Oscillations in adiabatic state populations

Our Min-Cost state reassignment algorithm [11] attributes new states in terms of old states allowing the diabatic pathway to be followed through the cross. This procedure is especially crucial in problems involving state crossings between two states spatially localized on different molecules (or different segments of a molecule), where the transition density localization of the current adiabatic state will undergo sudden unphysical changes when the two states cross [11]. Since the adiabatic state changes its character, artifacts of the back and forth crossings emerge and tracking the adiabatic state population loses physical meaning as state identities may frequently change. For example, the population of the adiabatic state $S_1^{(a)}$ is shown in the bottom panel of Figure 4 for each separation distance calculated as the fraction of trajectories evolving on the lowest energy adiabatic state at any given time. For the shortest separation distances, when there are no trivial unavoided crosses during the dynamics, the $S_1^{(a)}$ population steadily increases. On the other hand, when trivial unavoided

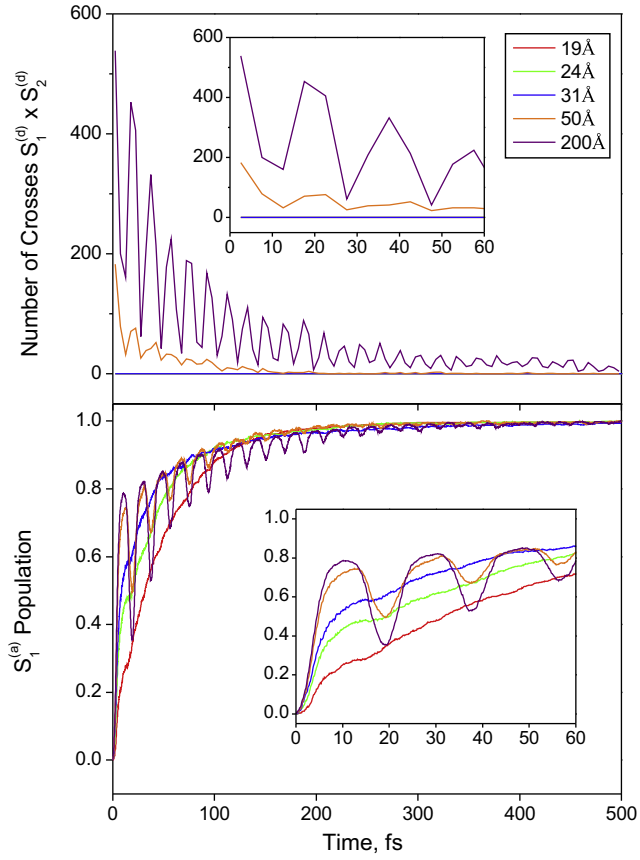

Figure 4. (Top) The total number of trivial unavoided crosses between $S_1^{(d)}$ and $S_2^{(d)}$ during the 500 fs dynamics for each separation distance. Trivial unavoided crossings appear for the largest separation distances, when the states become noninteracting. (Bottom) Population for the adiabatic $S_1^{(a)}$ state calculated as the fraction of trajectories in $S_1^{(a)}$ for each separation distance. For large separation distances (50 Å and 200 Å), oscillations in the population appear as a result of the trivial unadoided crossings.

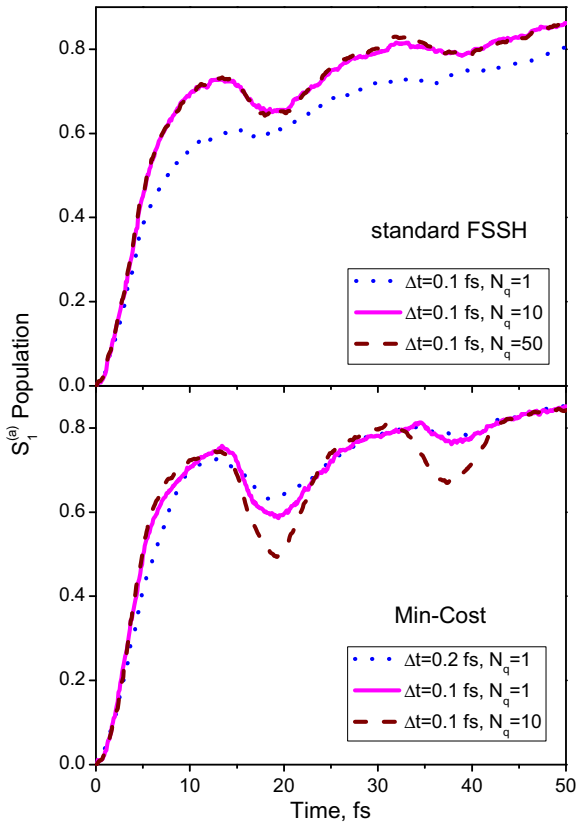

Figure 5. Short time NA-ESMD simulations of 3-ring and 4-ring PPV oligomers separated by 50 Å. Simulations are performed using different time steps (Top) using the standard FSSH algorithm (without the Min-Cost treatment) and (Bottom) with Min-Cost treatment of unavoided crossings.

crossings are present (50 Å and 200 Å), oscillations in the population appear. It is important to note that the minima of these oscillations correspond to the peaks in the number of crosses (top panel). The amplitude of the oscillations increases for the largest distance due to the larger number of crosses resulting in a large probability that $E_2^{(d)} < E_1^{(d)}$. Whenever $E_2^{(d)} < E_1^{(d)}$, the identity of $S_1^{(a)}$ changes and this is reflected as oscillations in the adiabatic state population. Finally, we observe that the quantum populations (not shown here), measured as the ensemble average of the quantum probability for a given state $\langle |c_i|^2 \rangle$, show similar oscillations since the quantum amplitudes are also interchanged between the crossing states.

Oscillations in the adiabatic state populations result from following the diabatic pathway through the cross. That can be achieved either by using Min-Cost state reassignment, or using standard FSSH without Min-Cost but with sufficiently small time steps. In the latter case, the finite time step prevents all unavoided crosses from being identified and inevitably some will be missed. In the limit of infinitely small time step, the standard FSSH result will reproduce the same oscillations observed in the Min-Cost simulations. This is obviously impractical. In principle, the oscillations should converge with the size of the propagation time step; Using Min-Cost, convergence should be achieved at a larger time step compared to standard FSSH, as can be seen in Figure 5 showing the $S_1^{(a)}$ population (fraction of trajectories) for the oligomers separated by 50 Å. Here, short time simulations were performed using different time steps without (top panel) and with (bottom panel) the Min-Cost treatment using 540 trajectories.

Oscillations are not present in the standard FSSH simulation with a large quantum time step $\delta t = 0.1$ fs ($\delta t = \Delta t / N_q$) (top panel, dotted line). A smaller time step of $\delta t = 0.01$ fs provides increased resolution of the NACT peaks [32], (top panel, solid line), and oscillations begin to appear as the standard FSSH algorithm identifies some unavoided crossings. However, even decreasing the timestep to $\delta t = 0.002$ fs (top panel, dashed line) does not provide any greater resolution. In the Min-Cost case, oscillations are present at the much larger time step of $\delta t = 0.2$ fs (bottom panel, dotted line) and are much stronger compared to the analogous standard FSSH simulations using the same time step (bottom panel, solid line $\delta t = 0.1$ fs; bottom panel, dashed line $\delta t = 0.01$ fs). Oscillations in the standard FSSH result signify that the system is experiencing unavoided crossings and that the Min-Cost treatment should be used. Unfortunately, this signal is not robust, since oscillations may be absent depending on the chosen simulation parameters. Therefore, it is essential to understand whether a system is in the interacting regime (simulated by quantum hops using standard FSSH) or noninteracting regime (requiring Min-Cost state reassignment).

4. Conclusion

In summary, our NA-ESMD simulation of coupled PPV oligomers shows that many of the initial states have mixed character at short distances being delocalized over both oligomers, which indicates strong interaction (Frenkel-type exciton). As the separa-

tion distance increases, the interaction between the states vanishes until a noninteracting regime is reached; for the largest separation distances, the excitations become localized to one segment. When noninteracting states occupy the same energy range, trivial unavoided crossings appear characterized by vanishing NACTs everywhere except at the exact moment of crossing, where they become infinitely large. Consequently, application of the Min-Cost state reassignment algorithm to allow tracking of the diabatic pathway through the cross is necessary. However, this leads to artifacts in the measured adiabatic state populations appearing as oscillations that correspond to the back and forth state crossings. In general, these oscillations are a consequence of treating trivial unavoided crossings correctly and following the diabatic pathway. Strong oscillations using the Min-Cost approach are an artifact of treating all of the unavoided crosses correctly, which can be achieved at a larger time step than if Min-Cost is not used. While oscillations would be removed if the population of the diabatic state (whose character does not change) could be tracked, instead of using adiabatic state populations, the changes in the transition density for the current state must be followed.

Acknowledgments

T. N. and S. T. acknowledge support of Directed Research and Development Fund at Los Alamos National Laboratory (LANL). A.E.R and S.F.-A. acknowledge supported from CONICET, UNQ, ANPC$_I$T (PICT-2010-2375), NSF Grants CHE-0239120 and CHE-0808910. Los Alamos National Laboratory is operated by Los Alamos National Security, LLC, for the National Nuclear Security Administration of the U.S. Department of Energy under contract DE-AC52-06NA25396. We acknowledge support of Center for Integrated Nanotechnology (CINT) and Center for Nonlinear Studies (CNLS).

References

[1] R.A. Mathies, C.H.B. Cruz, W.T. Pollard, C.V. Shank, Science 240 (1988) 777.
[2] J. Clark, T. Nelson, S. Tretiak, G. Cirmi, G. Lanzani, Nature Phys. 8 (2012) 225.
[3] M. Reufer, M.J. Walter, P.G. Lagoudakis, A.B. Hummel, J.S. Kolb, H.G. Roskos, U. Scher, J.M. Lupton, Nature Mater. 4 (2005) 340.
[4] W. Domcke, D.R. Yarkony, Annu. Rev. Phys. Chem. 63 (2012) 325.
[5] M.H. Kim, L. Shen, H.L. Tao, T.J. Martinez, A.G. Suits, Science 315 (2007) 1561.
[6] T.G. Goodson, Acct. Chem. Res. 38 (2005) 99.
[7] P. Peumans, S. Uchida, S.R. Forrest, Nature 425 (2003) 158.
[8] E. Collini, G.D. Scholes, Science 323 (2009) 369.
[9] G.D. Scholes, G.R. Fleming, A. Olaya-Castro, R. van Grondelle, Nature Chem. 3 (2011) 763.
[10] H. Lee, Y.-C. Cheng, G.R. Fleming, Science 316 (2007) 1462.
[11] S. Fernandez-Alberti, A.E. Roitberg, T. Nelson, S. Tretiak, J. Chem. Phys. 137 (2012) 014512.
[12] T. Nelson, S. Fernandez-Alberti, A.E. Roitberg, S. Tretiak, Phys. Chem. Chem. Phys. 15 (2013) 9245.
[13] T. Nelson, S. Fernandez-Aberti, V. Chernyak, A.E. Roitberg, S. Tretiak, J. Phys. Chem. B 115 (2011) 5402.
[14] J.C. Tully, J. Chem. Phys. 93 (1990) 1061.
[15] J.C. Tully, J. Chem. Phys. 137 (2012) 22A301.
[16] S. Tretiak, C. Isborn, A. Niklasson, M. Challacombe, J. Chem. Phys. 130 (2009) 054111.
[17] S. Tretiak, V. Chernyak, S. Mukamel, J. Chem. Phys. 105 (1996) 8914.
[18] F. Furche, R. Ahlrichs, J. Chem. Phys. 117 (2002) 7433.
[19] R. Send, F. Furche, J. Chem. Phys. 132 (2010) 044107.
[20] I. Tavernelli, B. Curchod, A. Laktionov, U. Rothlisberger, J. Chem. Phys. 133 (2010) 194104.
[21] S. Fernandez-Alberti, A.E. Roitberg, V.D. Kleiman, T. Nelson, S. Tretiak, J. Chem. Phys. 137 (2012) 22A526.
[22] M. Soler, A.E. Roitberg, T. Nelson, S. Tretiak, S. Fernandez-Alberti, J. Phys. Chem. A 116 (2012) 9802.
[23] S. Fernandez-Alberti, V.D. Kleiman, S. Tretiak, A.E. Roitberg, J. Phys. Chem. Lett. 1 (2010) 2699.
[24] S. Tretiak, S. Mukamel, Chem. Rev. 102 (2002) 3171.
[25] S. Mukamel, S. Tretiak, T. Wagersreiter, V. Chernyak, Science 277 (1997) 781.
[26] V. Chernyak, M.F. Schulz, S. Mukamel, S. Tretiak, E.V. Tsiper, J. Chem. Phys. 113 (2000) 36.
[27] M.J.S. Dewar, E.G. Zoebisch, E.F. Healy, J.J.P. Stewart, J. Am. Chem. Soc. 107 (1985) 3902.
[28] K. Drukker, J. Comput. Phys. 153 (1999) 225.
[29] M.P. Allen, D.J. Tildesley, Computer Simulations of Liquids, Claredon Press, Oxford, 1987.
[30] M.G. Paterlini, D.M. Ferguson, Chem. Phys. 236 (1998) 243.
[31] P. Attard, J. Chem. Phys. 130 (2009) 194113.
[32] T. Nelson, S. Fernandez-Aberti, V. Chernyak, A.E. Roitberg, S. Tretiak, J. Chem. Phys. 136 (2012) 054108.
[33] C. Wu, S.V. Malinin, S. Tretiak, V.Y. Chernyak, Nature Phys. 2 (2006) 631.
[34] S.N. Taraskin, S.R. Elliott, Phys. Rev. B 59 (1999) 8572.
[35] J.T. Edwards, D.J. Thouless, J. Phys. C Solid State Phys. 5 (1972) 807.
[36] R.J. Bell, P. Dean, D.C. Hibbins-Butler, J. Phys. C Solid State Phys. 4 (1970) 1214.